Divacancy in silicon: Hyperfine interactions from electron-nuclear double resonance measurements

de Wit, J.G.; Sieverts, E.G.; Ammerlaan, C.A.J.

DOI
10.1103/PhysRevB.14.3494

Publication date
1976

Published in
Physical Review. B, Condensed Matter

PHYSICAL REVIEW B VOLUME 14, NUMBER 8 15 OCTOBER 1976

Divacancy in silicon: Hyperfine interactions from electron-nuclear double resonance measurements

J. G. de Wit, E. G. Sieverts, and C. A. J. Ammerlaan
Natuurkundig Laboratorium der Universiteit van Amsterdam, Valckenierstraat 65, Amsterdam-C, The Netherlands
(Received 2 October 1975)

The Si-*G*6 EPR spectrum, which is associated with the positive charge state of the divacancy in silicon, was investigated by electron-nuclear double resonance. Hyperfine tensors describing the interaction between the unpaired divacancy electron and ^{29}Si nuclei were determined. With these results, detailed information about the wave function of the defect electron is gathered. Nearly all hyperfine tensors showed a distinct axial symmetry; for the majority the symmetry axis was along one of the ⟨111⟩ bond directions. A total number of 18 tensors was measured: 12 of these belong to a general class shell of atoms, the remaining 6 belong to a mirror-plane class shell. Thus the divacancy electron was probed in a region containing 60 atoms in the vicinity of the defect site. In agreement with a conclusion reported previously, the second largest general class interaction was identified with the nearest-neighbor general class shell of atoms. A complete matching of hyperfine tensors to specific shells of lattice sites was not possible without support by theoretical considerations.

I. INTRODUCTION

Among the defects produced in silicon by irradiation with energetic particles, the divacancy (V_2) is to date one of the best known centers. The divacancy is more conveniently studied than the monovacancy and the self-interstitial because, contrary to these simpler intrinsic defects, the divacancy is not mobile at room temperature. By electron irradiation of silicon at room temperature, divacancies are easily produced as stable and isolated centers, randomly distributed over the sample volume. Like many chemical impurities, divacancies introduce energy levels in the semiconductor band gap. Depending on the position of the Fermi level, the divacancy will assume a charge state ranging from singly positive in p-type to doubly negative in heavily doped n-type silicon. Owing to a single unpaired electron spin the divacancy is an $S = \frac{1}{2}$ paramagnetic center in both the V_2^+ and V_2^- charge states. The electron paramagnetic resonance (EPR) spectrum associated with the former state, which is the defect being studied here, was labeled Si-*G*6.[1] Several studies of the divacancy using EPR have been reported.[2-8] The present work draws heavily upon the existing knowledge of the divacancy, in particular the detailed information given by Watkins and Corbett.[4]

A divacancy is introduced in a silicon crystal by removing two atoms on adjacent lattice sites. A defect with this structure has point-group symmetry D_{3d} and can be oriented in the host lattice in four different ways, i.e., with its threefold axis along either of the four ⟨111⟩ bond directions. New bonds are formed by linear combination of the dangling bond orbitals residing on the six nearest neighbors of the divacancy. In this model the electronic ground state of the defect will be orbitally degenerate, and therefore be unstable against Jahn-Teller distortion. Such a distortion lowers the symmetry of the defect to C_{2h}, while the number of distinguishable orientations of the divacancy in the silicon lattice is increased to 12.

An important feature of the divacancy is the hyperfine interaction between the unpaired defect electron and the magnetic moments of neighboring ^{29}Si nuclei. The three largest hyperfine interactions, with ^{29}Si nuclei which are close neighbors of the divacancy, were already observed in[4] EPR; these interactions are labeled $M1$, $G1$, and $G2$ in this paper. An illustration taken from our own EPR spectra is given in Fig. 1. This result is representative of the best possible resolution obtainable by EPR, i.e., for a magnetic field direction along a high-symmetry crystal axis. Weaker hyperfine interactions are not resolved in EPR. They are the origin of inhomogeneous broadening of the resonance lines, which have a linewidth between 1 and 2 Oe [full width at half maximum (FWHM)]. Because of the inherent higher resolution, these weaker interactions are however readily separated using electron-nuclear double resonance (ENDOR).

The hyperfine interaction is expressed in the form of a tensor whose components are the hyperfine constants. The isotropic part of the interaction arises from Fermi contact interaction and is proportional to the probability density of the defect electron at the nuclear site. The anisotropic part is due to dipole-dipole coupling between the electronic and the nuclear magnetic moments. ENDOR

studies therefore reveal important information about the defect electron wave function.

Our present study is similar in scope to Hale and Mieher's investigation of the shallow donors P, As, and Sb in silicon.[9] In their paper, extending and updating early pioneering research by Feher,[10] an abundant number of hyperfine constants was reported. These data proved an ideal testing ground for the Kohn-Luttinger effective-mass theory.[11-22] Few other ENDOR studies have been performed on paramagnetic centers in silicon.[23-29]

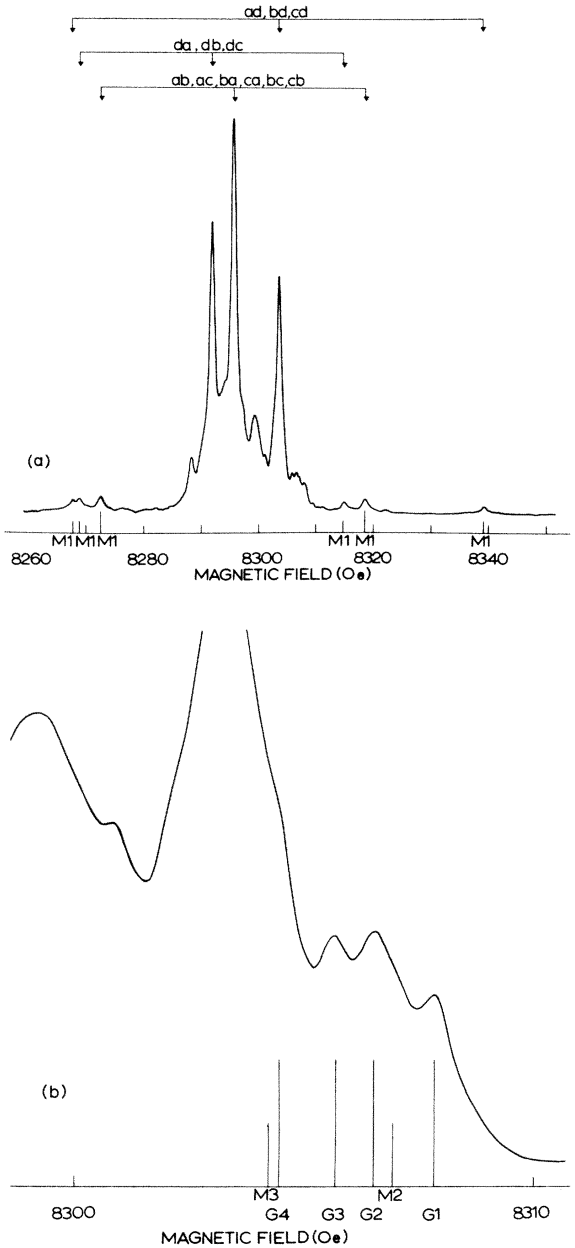

FIG. 1. Si-$G6$ EPR spectrum at 14 K and 23.249 GHz for $\vec{H}\|[111]$. (a) The whole spectrum including the largest hyperfine interaction $M1$; (b) an expanded part of the spectrum showing some of the weaker hyperfine interactions. Labels $M1$, $G1$, etc., refer to the hyperfine tensors.

II. EXPERIMENTAL PROCEDURE

Float-zoned single-crystalline silicon was purchased from Wacker-Chemitronic; all ingots were p type, doped with boron. A sample used for exploratory measurements had a preirradiation resistivity of 0.3 Ωcm and a dislocation density of about 2×10^4 cm^{-2}. The great majority of our experiments was however performed using a sample with an initial resistivity of 0.1 Ωcm and specified to be dislocation free. No differences in the results for the two batches were ever apparent.

Samples were subjected at room temperature to irradiation by 1.5 MeV electrons from a Van de Graaff accelerator. The bombardment current was kept below about 10 μA/cm^2 to avoid heating of the samples in excess of 50 °C. Optimum divacancy resonance signals required an electron fluence of 2×10^{18} electrons/cm^2, corresponding to a density of divacancies near 1.5×10^{16} cm^{-3}.[5] To improve the uniformity of the defect distribution, the electron fluence was divided in equal doses on each of two opposite sides of the samples. Samples were still p type after the irradiation, as was verified by measuring the sign of the thermoelectric power using a hot-point probe. The divacancies which were observed in EPR were thus thought to be in the positive charge state.

All magnetic resonance experiments were carried out in a superheterodyne spectrometer operating at 23 GHz. Klystron frequencies were synchronized to quartz crystal harmonics. The spectrometer was adjusted to observe the dispersion part of the EPR signal. A microwave power of 5 μW was incident upon the cavity. With a cavity quality factor $Q\simeq9{,}000$, this resulted in a microwave field amplitude $2H_1$ at the center of the sample position of 0.025 Oe. During ENDOR measurements, the sample temperature was kept at about 17 K. At this temperature the spin-lattice relaxation time T_1 of the divacancy equals 2.5×10^{-3} sec.[8] With this choice of conditions the EPR transition is strongly saturated, because the value of the saturation parameter is $\gamma_e H_1 T_1 = 600$. Temperatures were measured with a Au(0.03-at.% Fe)–Chromel thermocouple fastened to the cavity bottom and were kept constant within 0.1 K. A double audio-frequency modulation scheme followed by double phase-sensitive detection was used to obtain a simultaneous good presentation of EPR and ENDOR signal and a better noise reduction. As in

a conventional EPR experiment, the magnetic field was modulated sinusoidally at a frequency of 106 Hz and with an amplitude of 0.15 Oe. A 3.3-Hz square-wave modulation of the rf field was applied. The various parameters were optimized empirically in search for the best stationary ENDOR effect. In most cases this involved a compromise between narrow linewidths and large amplitudes; for the high-frequency resonances, linewidth considerations had to be sacrificed entirely in order to achieve an acceptable signal-to-noise ratio.

Our samples were cut and ground to obtain a nearly cylindrical shape. Typical sample dimensions were a height of 12 mm and a diameter of 1.7 mm. Samples were mounted with their axis along the axis of the cylindrical TE_{011} resonant cavity. A $\langle 110 \rangle$ crystallographic direction pointed vertically with an estimated error of less than 0.5 deg. For angular dependence studies the static magnetic field could be rotated in the horizontal plane, i.e., in a $\{110\}$ plane of the crystal. To introduce the rf field a coil assembly could be inserted in the cavity.[26] Two loops of fine copper wire forming a Helmholtz configuration and fixed to a thin-walled Teflon holder were then shifted over the sample.[30] This provided a rf field in the horizontal plane, which could be rotated perpendicular to the static field for maximum induction of the nuclear transitions. In another arrangement, use was made of a silver-coated Epibond cavity. A spiral groove was cut in the thin silver layer on the cylindrical side wall of the cavity to make this wall suitable as an ENDOR coil.[25] This setup produces a vertical rf magnetic field.

III. ANALYSIS OF DATA

A. Spin Hamiltonian

To analyze magnetic resonance spectra one conveniently relies upon a spin Hamiltonian incorporating all the relevant interactions. In the present case the Hamiltonian

$$\mathcal{H} = \mu_B \vec{H} \cdot \vec{g}_e \cdot \vec{S} - \mu_N g_N \vec{H} \cdot \vec{I}_\alpha + \vec{S} \cdot \vec{A}_\alpha \cdot \vec{I}_\alpha , \quad (1)$$

with an electronic Zeeman interaction term, one nuclear Zeeman term, and one hyperfine interaction term, respectively, was used to fit the experimental data. The parameter α enumerates the lattice sites around the divacancy. Each lattice site has a 4.7% probability of being occupied by a ^{29}Si isotope, which has a nuclear spin $I = \frac{1}{2}$ and a scalar nuclear g value, $g_N = -1.1095$. Both the hyperfine interaction and the electronic Zeeman effect are anisotropic, and have to be described by tensors. The electronic g tensor $\vec{g}_e$ is symmetric and has the components

$$g_{xx} = 2.0033, \quad g_{yy} = g_{zz} = 2.0016 ,$$

$$g_{xy} = g_{xz} = -0.0011, \quad g_{yz} = -0.0004 .$$

These components were derived from the principal values of the g_e tensor as given by Watkins and Corbett,[4] and are valid for the divacancy in the orientation with designation *ad*, and the coordinate system as defined in Fig. 2.

Anticipating the analysis of our results, the hyperfine interaction tensors $\vec{A}_\alpha$ are separated into a scalar part a_α and a traceless tensor $\vec{B}_\alpha$. Thus,

$$\vec{A}_\alpha = a_\alpha \cdot \vec{1} + \vec{B}_\alpha , \quad (2)$$

with $a_\alpha \equiv \frac{1}{3} \mathrm{Tr} \vec{A}_\alpha$ and $\mathrm{Tr} \vec{B}_\alpha = 0$. In this equation a_α describes the isotropic part of the interaction arising from the Fermi contact interaction.[31] The expression

$$a_\alpha = \tfrac{8}{3} \pi g_e \mu_B g_N \mu_N |\psi(\vec{r}_\alpha)|^2 \quad (3)$$

relates this hyperfine constant to the probability density of the defect electron at the nuclear site $\vec{r}_\alpha$. Dipole-dipole coupling between the electronic and nuclear magnetic moments is responsible for the anisotropic part in the interaction. Using the dipole-dipole interaction operator, one finds

$$(B_\alpha)_{ij} = g_e \mu_B g_N \mu_N \langle \psi | 3 r_i r_j / r^5 - \delta_{ij} / r^3 | \psi \rangle \quad (i,j = x,y,z) , \quad (4)$$

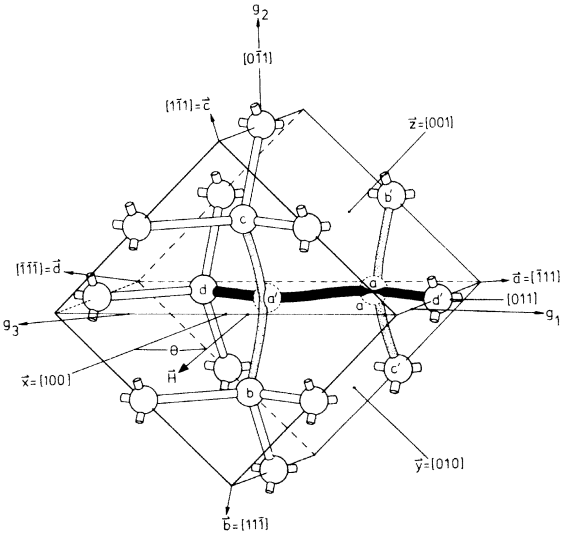

FIG. 2. Model of the divacancy at *aa'* in the orientation *ad*. The figure also shows the crystallographic directions, our choice of x,y,z coordinate system, the principal axes of the electronic g tensor of divacancy *ad*, and the plane in which the magnetic field $\vec{H}$ was varied in the ENDOR experiments. Jahn-Teller distortions of the lattice are not shown.

which shows the symmetry of the $\vec{\vec{B}}$ tensor.

A solution of the spin Hamiltonian eigenvalue problem is particularly easy in the limit of high magnetic field. In that case the electronic and nuclear magnetic moments are all parallel to the magnetic field with no breakdown of the quantization scheme. ENDOR transition frequencies are found by applying the selection rules $\Delta m_s = 0, \Delta m_{I\alpha} = \pm 1$, with the result

$$h\nu_\alpha^\pm = \left| g_N \mu_N H \pm \tfrac{1}{2} \hat{h} \cdot \vec{\vec{A}} \cdot \hat{h} \right| , \tag{5}$$

where $\hat{h}$ is a unit vector in the direction of the magnetic field $\vec{H}$. The two ENDOR frequencies arise from the two possible spin states of the electron, $m_s = \pm \frac{1}{2}$. The ENDOR spectrum is symmetric with respect to the nuclear Zeeman frequency $g_N \mu_N H/h$. For large hyperfine interactions a better approximation is required. A formula neglecting only terms of order $(A_\alpha)_{ij}^2/g_e \mu_B H$ and also taking the anisotropy of $\vec{\vec{g}}_e$ into account is

$$h\nu_\alpha^\pm = \left| g_N \mu_N \vec{H} \pm \tfrac{1}{2} \vec{\eta} \cdot \vec{A} \right| . \tag{6}$$

In this expression $\vec{\eta}$ is the unit vector $\vec{H} \cdot \vec{\vec{g}}_e / |\vec{H} \cdot \vec{\vec{g}}_e|$, specifying the electron-spin direction.

B. Symmetry considerations

1. Divacancy orientations

Before starting a discussion of the symmetry aspects we first define, by referring to Fig. 2, the x, y, z crystal coordinate system. A divacancy is introduced by removal of the atoms at the origin a' and at the nearest-neighbor site a. The coordinate system and the way of labeling divacancy orientations are identical to the method adopted by Watkins and Corbett.[4] In our analysis orientation *ad* of the divacancy is chosen as the basic orientation from which the properties of the other symmetry-related orientations are derived.

A perfect silicon crystal is generated by applying the operations of the space group $\mathcal{G} = Fd3m$. In a magnetic resonance experiment one does not distinguish between two defects which are transformed into each other by a pure translation. Therefore, it is sufficient for the present purposes to consider only the factor group $\mathcal{G}/\mathcal{J}$ with respect to the subgroup $\mathcal{J}$ of primitive translations. The order $O(\mathcal{G}/\mathcal{J})$ of the factor group is 48.

Some of the symmetry operations of the crystal leave a divacancy invariant. More specifically, using the conventional notation {(im)proper rotation | translation}, the divacancy in the orientation *ad* remains unchanged under the identity $\{E|0\}$, the reflection $\{\sigma_{d(0\bar{1}1)}|0\}$, the inversion $\{\bar{i}|\frac{1}{4}a(\bar{1},1,1)\}$, and the twofold rotation $\{i\sigma_{d(0\bar{1}1)}|\frac{1}{4}a(\bar{1},1,1)\}$. Together these four covering operations of the divacancy *ad* form a subgroup $\mathcal{S}$ of order $O(\mathcal{S}) = 4$.

The number of distinguishable divacancy orientations is equal to $O(\mathcal{G}/\mathcal{J})/O(\mathcal{S}) = 12$.

2. Shells

By applying the operations of $\mathcal{S}$ on a ^{29}Si atom at a general position in the lattice, a shell of symmetry-related lattice sites is generated. An example of a shell around the divacancy in orientation *ad* is given by the four sites labeled b, c, b', and c' in Fig. 2. On a larger scale, the 48 symmetry-related lattice sites belonging to all 12 different divacancy orientations is called a supershell.

Equation (1) describes the interaction of a divacancy in the orientation *ad* with one ^{29}Si nucleus. From Eq. (1) 47 symmetry-related Hamiltonians are derived by appropriate transformations. As inversion produces no new results, only 24 different Hamiltonians are obtained. For one supershell we therefore expect an ENDOR spectrum consisting of 24 low-frequency and 24 high-frequency lines.

3. Classes

For a ^{29}Si atom on a general lattice site, the operations of $\mathcal{S}$ generate a four atom shell. If however the initial lattice site is on the mirror plane of the divacancy, then the shell contains only two atoms, as the reflection produces no new results. The atoms d and d' in Fig. 2 are an example of this situation. We therefore distinguish between general class shells and mirror-plane class shells.

For a divacancy with a ^{29}Si atom on a mirror-plane position, the spin Hamiltonian must be invariant under the reflection operation. For the hyperfine tensors, the restrictions this imposes on their most general form are $A_{yy} = A_{zz}$ and $A_{xy} = A_{xz}$. The number of independent components for a general class tensor is six, for a mirror-plane class tensor this number is reduced to four. A summary of shell properties is given in Table I.

4. Patterns

It was shown that for a general direction of the magnetic field $\vec{H}$ the number of ENDOR lines on each side of the nuclear Zeeman frequency is 24 for a general class supershell, while it is only 12 for a mirror-plane class supershell. For $\vec{H}$ in a {110} plane, as in our experiments, some resonance frequencies will coincide. Still more symmetry-required degeneracy will occur for $\vec{H}$ along the low index directions [100], [111], and [011]. The ENDOR transition frequencies at these partic-

TABLE I. Properties of shells.

	General class	Mirror-plane class
^{29}Si site location (n_x,n_y,n_z) for divacancy orientation *ad*.	$n_y \neq n_z$	$n_y = n_z$
Number of sites in supershell	48	24
Number of sites in shell	4	2
Number of independent hyperfine tensor components	6	4

ular directions of $\vec{H}$ are labeled by S_i, T_i, and U_i, respectively. The angular dependence of all ENDOR lines of a supershell taken together form a characteristic pattern, with distinct differences between general class and mirror-plane class supershells. Information on the properties of patterns is given in Table II.

C. Reduction of data

1. Experimental results

Two of the experimentally recorded ENDOR spectra are reproduced in Figs. 3 and 4. In the first of these figures the central region of a spectrum is displayed. The symmetrical appearance of the ENDOR lines with respect to the nuclear Zeeman resonance frequency at 6.891 MHz is demonstrated. In Fig. 4 a smaller part of a spectrum more slowly swept, is presented to show the resolution. Although in some cases lines as narrow as 3 kHz could be obtained, a linewidth (FWHM) of about 10 kHz is more typical for most experiments. Spectra for a high-symmetry crystal direction are shown because then the number of ENDOR lines is smallest and the separation of the lines is best.

The angular dependence of the spectra was taken by rotating the magnetic field in the $(0\bar{1}1)$ plane of the sample, from $\theta = 0°$ for $\vec{H} \| [100]$ to $\theta = 90°$ for $\vec{H} \| [011]$ (Fig. 2). Severe overlap between lines in various parts of the spectra forced us to use a fine network of angular settings in order to be able to unravel the patterns. Normally the spectrum was recorded at every 10° in the interval $0° \leq \theta \leq 90°$ on all EPR lines of the divacancy. In difficult parts of the spectrum, data were taken at 5° intervals, occasionally at 2° intervals. The ENDOR lines were measured on the high-frequency side of the nuclear Zeeman frequency. All of the spectra recorded on the low-frequency side, confirmed the symmetry with respect to the center of the ENDOR spectrum.

The angular dependence of ENDOR frequencies reveals the characteristic patterns of the general and the mirror-plane class supershells. The hyperfine interaction patterns of the $G10$ general class and of the $M5$ mirror-plane class supershells are shown as examples in Figs. 5 and 6, respectively. In the latter case the frequencies S_1 and S_2, T_2 and T_4, U_1 and U_5, and U_2 and U_6 are nearly equal, which is an indication of the approximate $\langle 111 \rangle$ axial symmetry of this interaction. Labels along the curves specify the divacancy orientations for which the ENDOR transitions are observable, while the degeneracy of the line is noted in parentheses. Drawn lines were calculated from the least-squares adjusted hyperfine tensor components. The dots represent experimental S, T, and U values, the number of which in all cases agrees with the specifications given in Table II.

A total of 18 hyperfine interaction tensors was measured and analyzed. Of these, 12 belong to

TABLE II. Properties of patterns.

	General supershell	Mirror-plane supershell
Number of ENDOR lines at general angle	24	12
Number of ENDOR lines at general angle in {110} plane	12	7
Number of S values	3	2
Number of T values	4	3
Number of U values	6	4

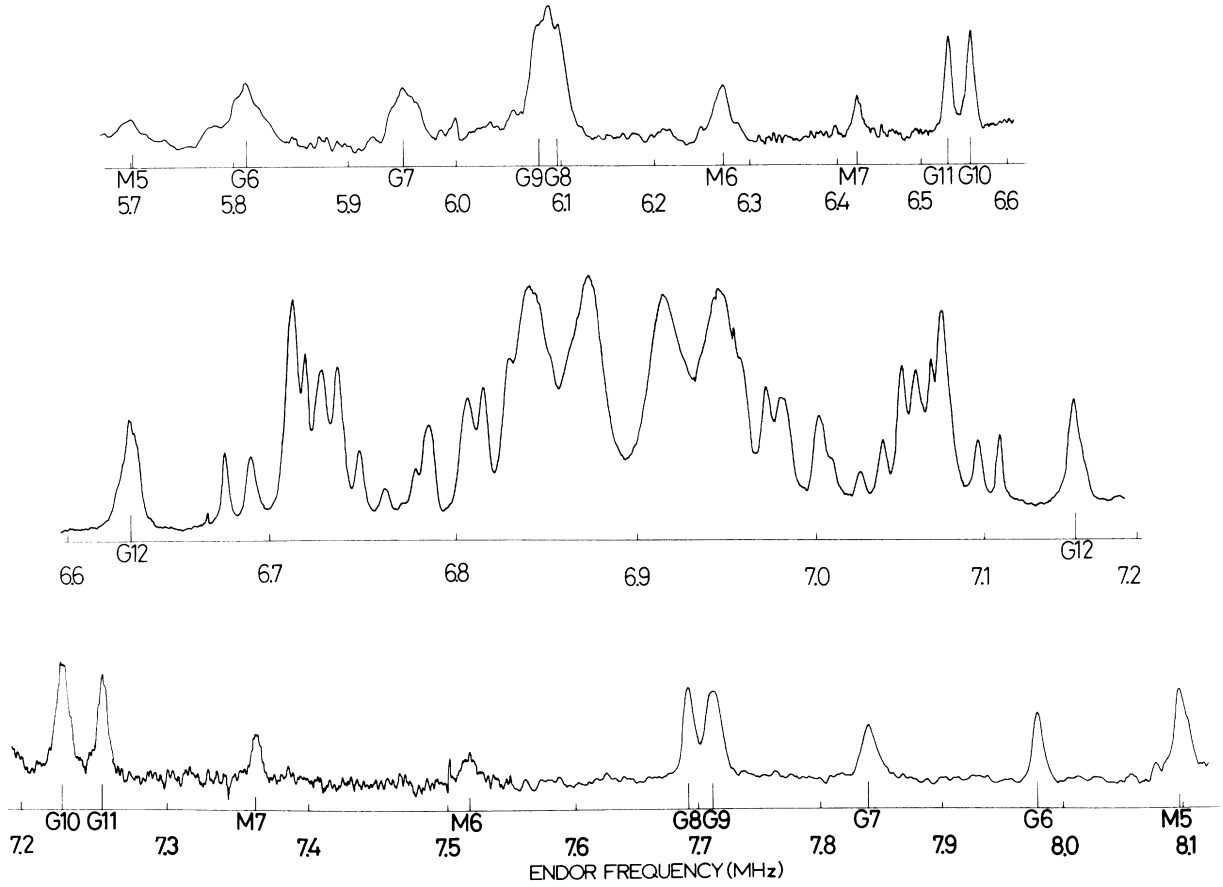

FIG. 3. Recorder trace of the divacancy ENDOR spectrum with $\vec{H}$ along the [100] crystal direction. The low-field EPR transition, associated with the divacancy orientations *ad*, *da*, *bc*, and *cb* was saturated. Labels assigned to the lines correspond with the labels given to the tensors in Table III. The central frequency equals 6.891 Mhz.

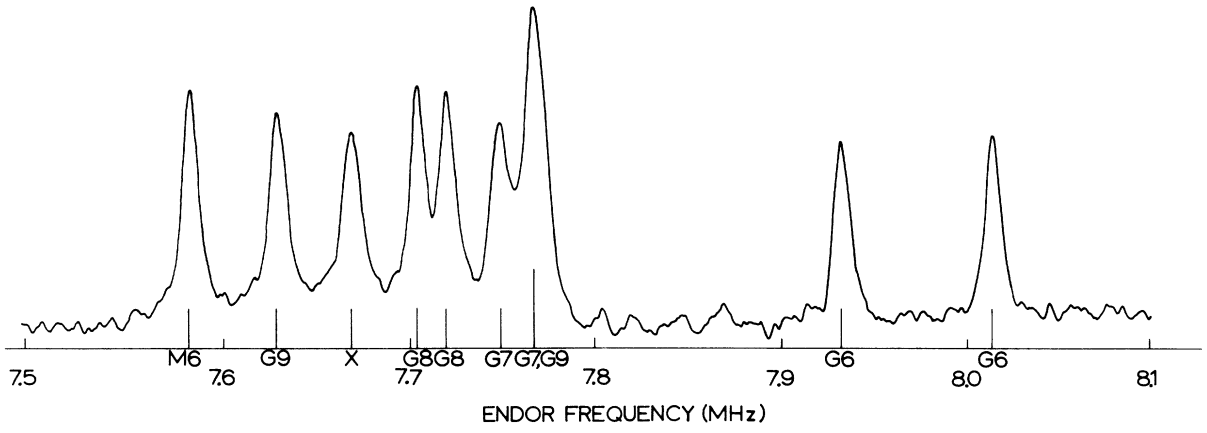

FIG. 4. Small part of the divacancy ENDOR spectrum for $\vec{H} \| [100]$ and for the high-field EPR transition, associated with the divacancy in the orientations *ab*, *ac*, *ba*, *ca*, *bd*, *cd*, *db*, and *dc*.

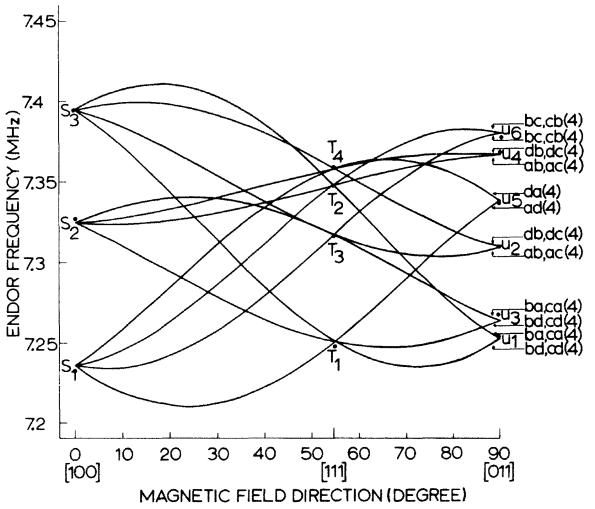

FIG. 5. Angular dependence of the ENDOR frequencies for the $G10$ shells, shown as an example of a general class interaction.

the general class of tensors which were given the names $G1$, etc. The remaining six tensors belonged to the mirror-plane class and were labeled $M2$, etc. The hyperfine tensor components of $M1$, describing the largest interaction, were taken from EPR data of Watkins and Corbett,[4] who also reported the isotropic part of the tensors $G1$ and $G2$. Many more hyperfine interactions were clearly present in the regions between 100 and 200 kHz above and below the central frequency. These interactions, corresponding to at least five shells, are not yet analyzed owing to severe overlapping of lines.

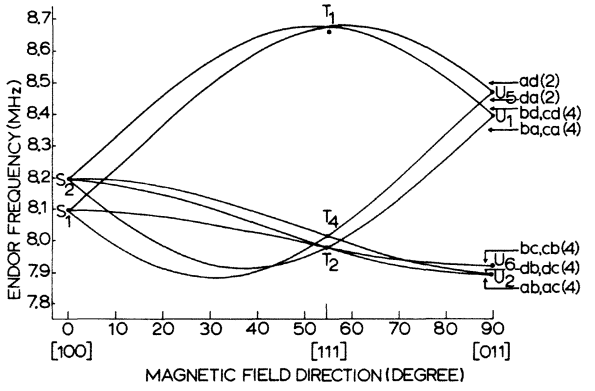

FIG. 6. Angular dependence of the ENDOR frequencies for the $M5$ shells, shown as an example of a mirror-plane class interaction, which moreover has also nearly ⟨111⟩ axial symmetry.

2. Tensor components

By the complete angular dependence studies sets of related S, T, and U values are sorted out. To calculate the tensor components only the S, T, and U values of a pattern were used. To inspect the closeness of the final fit and to avoid false interpretations the calculated patterns were afterwards compared with the experimental ones. There are always more than twice as many S, T, and U values as there are independent tensor components. Therefore a least-squares-fitting procedure was adopted. For most tensors the high-field approximation is applicable. In such cases the least-squares-fitting procedure is particularly easy as the ENDOR frequencies are linearly related to the hyperfine components. Explicit formulas expressing the hyperfine components in terms of S, T, and U values can be derived.[32] However, the high-field approximation is not always sufficiently accurate. Therefore the results for all tensors were subjected to a computerized least-squares adjustment. This procedure involved diagonalization of the full spin Hamiltonian [Eq. (1)], including the anisotropic electronic g tensor, a scalar nuclear g_N value, and only one ^{29}Si hyperfine interaction. Second-order hyperfine interactions were not taken into account. Symmetric tensors were used, although for the divacancy, a center of monoclinic symmetry, a more general form of tensor is allowed.[33-35] Interactions leading to asymmetry of the tensors are negligibly small, as the orbital angular momenta in silicon are effectively quenched, and they enter only in second order. The hyperfine components as determined by using the high-field expressions served as well-chosen starting parameters in the iterative numerical calculations.

Results for the hyperfine tensor components, expressed in the x,y,z crystal coordinate system (Fig. 2), are given in columns 2–7 of Table III. They are appropriate for the divacancy in orientation *ad*. As described in Sec. III A, a separation into an isotropic part a and an anisotropic tensor $\vec{\vec{B}}$ with $\mathrm{Tr}\vec{\vec{B}}=0$ was made. For the mirror-plane class tensors, symmetry requires $B_{yy}=B_{zz}$ and $B_{xy}=B_{xz}$. By suitable rotations the tensors were transformed to their own principal-axes systems. Principal values and directions of the principal axes are also given in Table III. The three principal values are called A_1, A_2, and A_3 in order of descending magnitude. Directions are specified by the two angles γ_i and δ_i, where γ_i is the angle between the ith eigenvector and its projection on the $(0\bar{1}1)$ plane and the angle between this projection and the [100] axis is δ_i. For a mirror-plane class tensor it follows from symmetry that one of

TABLE III. Experimental results for the hyperfine interaction tensor components for the positive divacancy in silicon.

Shell	a (MHz)	B_{yy} (MHz)	B_{zz} (MHz)	B_{xy} (MHz)	B_{xz} (MHz)	B_{yz} (MHz)
General class						
$G1$	22.53	−1.27	−0.53	1.73	2.13	1.08
$G2$	19.17	−0.10	0.44	−0.17	−0.85	−0.79
$G3$	10.18	0.26	−0.23	1.57	1.55	1.69
$G4$	7.05	−0.11	0.15	−0.97	1.02	−1.04
$G5$	3.548	−0.215	0.423	0.004	0.469	−0.180
$G6$	2.142	−0.086	0.075	0.332	0.350	0.322
$G7$	1.775	−0.067	−0.041	−0.362	0.286	−0.278
$G8$	1.606	−0.003	0.027	−0.236	0.254	−0.257
$G9$	1.594	−0.142	0.121	0.188	0.284	0.215
$G10$	0.835	0.013	0.152	−0.057	−0.103	−0.042
$G11$	0.602	−0.064	−0.058	0.098	0.070	0.040
$G12$	0.532	−0.011	0.017	0.091	0.075	0.077
Mirror-plane class						
$M1$[a]	147.7	B_{zz}	0.3	B_{xz}	27.6	28.1
$M2$	14.87	B_{zz}	0.14	B_{xz}	2.89	2.50
$M3$	5.423	B_{zz}	0.195	B_{xz}	−0.782	1.026
$M4$	3.151	B_{zz}	−0.301	B_{xz}	0.302	0.098
$M5$	2.516	B_{zz}	0.067	B_{xz}	0.492	0.543
$M6$	1.320	B_{zz}	0.040	B_{xz}	−0.208	0.260
$M7$	0.977	B_{zz}	0.024	B_{xz}	−0.038	−0.073

Shell	A_1 (MHz)	A_2 (MHz)	A_3 (MHz)	γ_1 (deg)	δ_1 (deg)	γ_2 (deg)	Axial direction
$G1$	26.40	20.75	20.44	−4.4	36.8	28.5	
$G2$	20.42	19.13	17.96	61.4	−35.5	−28.4	
$G3$	13.39	8.72	8.42	2.5	55.8	−28.9	d
$G4$	9.08	6.08	5.99	−55.7	4.2	24.8	b,c
$G5$	4.248	3.337	3.060	−47.7	47.8	41.8	
$G6$	2.817	1.842	1.767	−4.1	54.0	48.7	d
$G7$	2.403	1.513	1.408	−48.5	−2.3	33.7	b,c
$G8$	2.105	1.361	1.351	−56.5	2.7	9.0	b,c
$G9$	2.083	1.378	1.322	−11.5	53.1	32.2	d
$G10$	1.021	0.864	0.620	51.2	−65.8	−38.9	
$G11$	0.792	0.521	0.493	3.1	29.3	30.4	
$G12$	0.694	0.470	0.432	−1.2	55.1	55.9	d
$M1$	203	120	120	0	55.2	...	d
$M2$	20.39	12.52	11.70	0	54.8	90	d
$M3$	7.207	4.592	4.470	0	−63.0	90	a
$M4$	3.937	2.764	2.752	0	23.4	0	
$M5$	3.543	2.040	1.966	0	59.1	90	d
$M6$	1.780	1.100	1.079	0	−61.5	90	a
$M7$	1.074	0.983	0.875	90	...	0	

[a] From EPR data (Ref. 4).

the principal axes is parallel to $[0\bar{1}1]$, i.e., $\gamma_i = 90°$. The other two eigenvectors are in the $(0\bar{1}1)$ plane, i.e., $\gamma_j = \gamma_k = 0°$, and also $|\delta_j - \delta_k| = 90°$.

From the ENDOR data no unique assignment of a hyperfine tensor with the $\{E|0\}$ and $\{i|\frac{1}{4}a(\bar{1},1,1)\}$ sites of a general class shell on the one hand, or with the $\{\sigma_{d(0\bar{1}1)}|0\}$ and $\{i\sigma_{d(0\bar{1}1)}|\frac{1}{4}a(\bar{1},1,1)\}$ sites of such a shell on the other hand, can be made. This implies that for general class tensors in the crystal coordinate system a simultaneous interchange of B_{yy} with B_{zz} and of B_{xy} with B_{xz} is allowed. In the principal axes system the equivalent statement

is that a simultaneous change of the signs of all γ_i is allowed. This ambiguity problem does not arise for mirror-plane class tensors.

3. *Error limits*

In the experimental spectra the typical width of the resonances was about 10 kHz measured at half maximum (FWHM). Line positions could therefore be determined with an uncertainty of less than 2 kHz. Average deviations in comparing experimental values with calculated ones after least-squares adjustment of the hyperfine parameters were also generally within 2 kHz. Owing to signal-to-noise problems and increase in linewidth an absolute error of 10 kHz is given for the $G1$–$G4$ tensors. For tensor $M2$ these experimental problems were still larger resulting in an estimated error of 1%. Finally for the tensor $M1$ the hyperfine components, which were derived from EPR data, have a possible error of less than 3%.

In the least-squares-fitting procedure the anisotropy of the g_e tensor was taken into account. This, however, is not of much practical importance as the anisotropy is smaller than the accuracy of about 0.5° which was achieved in the alignment of the sample crystallographic axes with respect to the magnetic field.

IV. DISCUSSION OF RESULTS

A. Hyperfine axes

By inspection of Table III it becomes clear that for most hyperfine tensors the principal values A_2 and A_3 are nearly equal and smaller than A_1. The notable exceptions are the tensors $G2$, $G10$, and $M7$. The other 16 tensors therefore describe an interaction which is nearly axially symmetric around the axis of the $\vec{A}_1$ eigenvector of the tensor. It appears that for 12 of these 16 tensors the direction of axial symmetry almost coincides with one of the ⟨111⟩ bond directions of the silicon crystal lattice. The axial directions, in the adopted system of labeling them by a, b, c, and d (Fig. 2), are specified in the last column of Table III. A summary of the directional properties of all the tensors is given in Table IV.

This result suggests that for the divacancy in its positive charge state the unpaired electron around the defect is accommodated in the directed orbitals between pairs of neighboring atoms. A wave function for this electron may be constructed by forming a linear combination of atomic $3s$ and $3p$ orbitals centered on various atoms around the defect. The s part of the wave function with respect to a specific lattice site is proportional to the isotropic part of the corresponding hyperfine tensor, as is expressed by Eq. (3). From the dipole-dipole interaction the p part of the wave function may be obtained using Eq. (4). Such an analysis indicates that, for the 12 tensors considered, the wave function has only about 13% s character and 87% p character. Therefore a significant deviation occurs from the sp^3 hybridized character of the covalent bonds. This spoils the simple picture of a hole residing in the otherwise unperturbed bonds in the vicinity of the defect. A more detailed study of the defect electron wave function will be given in a future paper.

B. Motional effects

Identification of the hyperfine tensors with specific lattice shells is one of the major problems left. From the experimental data, as discussed hitherto, only a broad division in tensors corresponding with general class shells and tensors for mirror-plane class shells could be made. However, one more useful piece of experimental information is available. At elevated temperatures, above $\simeq 110$ K, the jump rate of the divacancy between the members of a triplet of Jahn-Teller configurations with a common vacancy-vacancy axis, e.g., ab, ac, and ad, is so high that motionally averaged resonance spectra are observed.[4] Effectively this implies a lifting of the Jahn-Teller distortion, with a corresponding

TABLE IV. Directional properties of hyperfine interaction tensors.

	Number of tensors	
	General class	Mirror-plane class
Total	12	7
$A_1 \neq A_2 \neq A_3$	2	1
Axial symmetry	10	6
⟨111⟩ axial symmetry	7	5
$\vec{A}_1 \parallel \vec{a} = [\bar{1}11]$	0	2
$\vec{A}_1 \parallel \vec{b} = [11\bar{1}]$ or $\vec{c} = [1\bar{1}1]$	3	...
$\vec{A}_1 \parallel \vec{d} = [\bar{1}\bar{1}\bar{1}]$	4	3

increase of the point-group symmetry from the distorted C_{2h} to the original D_{3d}. A whole new classification in terms of shells and classes is required to describe this properly. One of the new classes is again a {110} mirror-plane class. However, a shell of this class now contains six atoms, and is constructed by taking together one general shell and one mirror-plane shell of the previously discussed C_{2h} symmetry. An example of a point-group D_{3d} mirror-plane class shell are the nearest-neighbor atoms b, c, d, b', c', and d' of the divacancy (Fig. 2).

In the motionally averaged state the hyperfine interaction experienced by the defect electron is an average of the original values. Watkins and Corbett[4] observed a motionally averaged splitting of 22.4 Oe for $\vec{H}=7140$ Oe and $\vec{H}\|[100]$. An interaction of this magnitude can only be explained when the largest mirror-plane interaction $M1$ and one of the larger general class interactions is involved in the averaging. Three cases have to be considered depending on whether the ^{29}Si nucleus is located on the positions b or b', c or c', or d or d'. The differences in the hyperfine splittings calculated for these three cases are less than 0.5 Oe, and will not be resolved in EPR. Therefore only one line at the average position is observed. By averaging over the hyperfine atom position, at the same time the ambiguity due to the y,z equivalence, discussed in Sec. III C 2, is eliminated. The hyperfine splittings for the conditions mentioned above for the experiment reported in Ref. 4 were calculated. The results, taking into account the anisotropic form of the tensors, are 23.6, 22.7, and 21.2 Oe for $G1$, $G2$, and $G3$, respectively. The best match therefore is obtained when averaging $M1$ and $G2$, which implies that $M1$ and $G2$ constitute a D_{3d} shell. No doubt the interaction described by $M1$ originates from a ^{29}Si nucleus on the site d or d'. From this we conclude that $G2$ is the hyperfine interaction tensor for the general class shell of atoms b, c, b', and c', thus confirming the identification that was made earlier.[4]

ACKNOWLEDGMENTS

The authors are grateful to Dr. J. Wolfrat for his participation in the experiment. This work received financial support from the Foundation for Fundamental Research of Matter (F.O.M.).

[1]G. D. Watkins, *Radiation Damage in Semiconductors* (Dunod, Paris, 1965), p. 97.
[2]J. W. Corbett and G. D. Watkins, Phys. Rev. Lett. 7, 314 (1961).
[3]G. Bemski, B. Szymanski, and K. Wright, J. Phys. Chem. Solids 24, 1 (1963).
[4]G. D. Watkins and J. W. Corbett, Phys. Rev. 138, A543 (1965).
[5]J. W. Corbett and G. D. Watkins, Phys. Rev. 138, A555 (1965).
[6]C. A. J. Ammerlaan and G. D. Watkins, Phys. Rev. B 5, 3988 (1972).
[7]J. G. de Wit, C. A. J. Ammerlaan, and E. G. Sieverts, *Lattice Defects in Semiconductors* (The Institute of Physics, London, 1975), p. 178.
[8]C. A. J. Ammerlaan and A. van der Wiel, J. Magn. Reson. 21, 387 (1976).
[9]E. B. Hale and R. L. Mieher, Phys. Rev. 184, 739 (1969).
[10]G. Feher, Phys. Rev. 114, 1219 (1959).
[11]W. Kohn and J. M. Luttinger, Phys. Rev. 98, 915 (1955).
[12]J. M. Luttinger and W. Kohn, Phys. Rev. 97, 869 (1955).
[13]W. Kohn, *Solid State Physics*, edited by F. Seitz and D. Turnbull (Academic, New York, 1957), Vol. 5, p. 257.
[14]E. B. Hale and R. L. Mieher, Phys. Rev. 184, 751 (1969).
[15]E. B. Hale and R. L. Mieher, Phys. Lett. A 29, 350 (1969).
[16]E. B. Hale and T. G. Castner, Jr., Phys. Rev. B 1, 4763 (1970).
[17]T. G. Castner, Jr., E. B. Hale, and R. Craven, *Proceedings of the Tenth International Conference on Physics of Semiconductors, Cambridge, Mass., 1970,* edited by S. P. Keller, J. C. Hensel, and F. Stern (U.S.A.E.C., Oak Ridge, Tenn., 1970), p. 613.
[18]T. G. Castner, Jr., Phys. Rev. B 2, 4911 (1970).
[19]E. B. Hale and R. L. Mieher, Phys. Rev. B 3, 1955 (1971).
[20]J. L. Ivey and R. L. Mieher, Phys. Rev. Lett. 29, 176 (1972).
[21]J. L. Ivey and R. L. Mieher, Phys. Rev. B 11, 822 (1975).
[22]J. L. Ivey and R. L. Mieher, Phys. Rev. B 11, 849 (1975).
[23]G. D. Watkins and F. S. Ham, Phys. Rev. B 1, 4071 (1970).
[24]G. W. Ludwig, Phys. Rev. 137, A1520 (1965).
[25]H. H. Woodbury and G. W. Ludwig, Phys. Rev. 117, 102 (1960).
[26]G. D. Watkins and J. W. Corbett, Phys. Rev. 134, A1359 (1964).
[27]G. D. Watkins, Phys. Rev. 155, 802 (1967).
[28]E. L. Elkin and G. D. Watkins, Phys. Rev. 174, 881 (1968).
[29]K. L. Brower, Phys. Rev. B 1, 1908 (1970).
[30]H. Seidel, Z. Phys. 165, 218 (1961).
[31]E. Fermi, Z. Phys. 60, 320 (1930).
[32]J. G. de Wit, thesis (University of Amsterdam, 1975) (unpublished).
[33]F. K. Kneubühl, Phys. Kondens. Mater. 1, 410 (1963).
[34]F. K. Kneubühl, Phys. Kondens. Mater. 4, 50 (1965).
[35]A. Bieri and F. K. Kneubühl, Phys. Kondens. Mater. 4, 230 (1965).